N94- 29658

TDA Progress Report 42-116 February 15, 1994

A Dual-Cavity Ruby Maser for the Ka-Band Link Experiment

J. Shell and R. B. Quinn
Radio Frequency and Microwave Subsystems Section

A 33.68-GHz dual-cavity ruby maser was built to support the Ka-Band Link Experiment (KABLE) conducted with the Mars Observer spacecraft. It has 25 dB of net gain and a 3-dB bandwidth of 85 MHz. Its noise temperature referred to the cooled feedhorn aperture is 5 K.

I. Introduction

The purpose of this article is to describe the design, construction, and performance of a dual-cavity ruby maser used to support the first Ka-band telemetry downlink demonstration from a spacecraft in deep space. The Ka-band downlink from the Mars Observer spacecraft was at either 33.6709 or 33.6926 GHz. The low transmitted-signal level necessitated that the best possible receiver sensitivity be available. (The link margin for the Ka-band signal was estimated to be 1.6 dB, whereas the margin for the X-band (approximately 8.4-GHz) signal was estimated to be 38.2 dB). Therefore, a low noise temperature for the maser was a primary goal. This was achieved by operating the maser between 1.5 and 1.6 K physical temperature and including the feedhorn and other feed components in the cryogenic package.

Since the two possible downlink frequencies differ by only 22 MHz, a center frequency of 33.68 GHz was selected, and the design goal was to achieve sufficient instantaneous bandwidth to receive either frequency without retuning the maser. Since broad tunability was not a requirement, and the instantaneous bandwidth requirement was fairly narrow, a waveguide cavity design was chosen to give the best performance for the least complexity.

The maser package utilizes superfluid helium in a commercial cryogenic dewar with superinsulation. This package was not intended to tilt and was mounted in a stationary, vertical position in the pedestal room of the 34-m DSS-13 beam waveguide antenna.

II. General Design Considerations

The first parameter to be determined in the design of a cavity maser is the number of cascaded cavities. The total maser gain need only be large enough that the noise contribution from the follow-up high electron mobility transistor (HEMT) amplifier is not significant. For example, with a HEMT amplifier noise temperature of 40 K, a maser net gain of 25 dB results in a HEMT amplifier contribution to the total front-end amplifier noise temperature of 0.13 K. If the maser net gain is 25 dB, the ruby electronic gain will need to be several dB more to overcome losses in the

maser cavities, isolators, filters, and connecting waveguide. The estimated necessary ruby electronic gain was approximately 28 dB.

A. Gain Stability

One of the primary concerns in determining the required number of cavities is the gain stability. The fewer the number of cavities, the higher the required gain per cavity. Higher gain implies less stability because, to achieve a power gain of 100 or more in a single cavity, you must operate close to the onset of oscillation.

A rough estimate of the gain stability of the maser as a function of the bath temperature can be obtained in the following way: The temperature dependence of the gain of the maser is determined by the temperature dependence of the magnetic Q, Q_m. The magnetic Q is a useful quality factor in determining the gain of a maser. It quantifies the ability of a maser material, such as ruby, to amplify a signal. In circuit terms, it describes how heavily the "spins" (magnetic moments associated with the chromium ions in the ruby) load the cavity circuit. (For a thorough explanation of the maser process and definitions of terms used to explain the process, the reader should refer to Siegman [1] or other appropiate material.)

Q_m has two temperature dependent factors, the inversion ratio, I, and the thermal equilibrium spin population. (The inversion ratio is the ruby electronic gain in dB divided by the ruby absorption in dB.) For ruby oriented at the push–pull angle of 54.735 deg, the thermal equilibrium spin population is essentially independent of temperature at 1.5 K, and its variation will not be considered. Earlier theoretical work [2] suggests that the temperature dependence of the inversion ratio varies as

$$I \propto T^{-0.7} \tag{1}$$

for 1.5 K $< T <$ 2 K. Since Q_m is inversely proportional to the inversion ratio [1], Q_m must vary as

$$Q_m \propto T^{0.7} \tag{2}$$

The power gain ratio of a maser cavity at resonance is given by

$$G = \left| \frac{Q_m + Q_e}{Q_m - Q_e} \right|^2 \tag{3}$$

where Q_e is the external cavity Q. A more general expression will be given later. Solving for the ratio of the Q's gives

$$\frac{Q_e}{Q_m} = \frac{\sqrt{G} - 1}{\sqrt{G} + 1} \tag{4}$$

For example, a single cavity with 28 dB (ratio of 630.96) of gain requires a Q_e/Q_m ratio of 0.9234. Assuming a bath temperature of 1.55 K,

$$\frac{(Q_e/Q_m)_{T=1.54}}{(Q_e/Q_m)_{T=1.55}} = \left(\frac{1.55}{1.54}\right)^{0.7} = 1.00454 \tag{5}$$

Therefore, $(Q_e/Q_m)_{T=1.54}$ will be (1.00454)(0.92343) = 0.927623. Putting this new value into Eq. (3) yields a gain of 709.33, or 28.51 dB. Thus, a 0.01-deg bath temperature change will result in a 0.51-dB gain change if all the gain comes from one cavity. Similar calculations have been done for two, three, and four cavities. These results are shown in Table 1. There is a significant reduction in gain variation going from one to two cavities, but further improvement in going to three or four cavities is small. Therefore, a two-cavity design offers significantly better gain stability without adding considerably more complexity.

B. Bandwidth

Siegman [1] has compared the bandwidth of the traveling wave maser and the "ideal" cavity maser. An ideal cavity maser has a magnetic Q much smaller than the atomic Q. (This will be shown shortly to be the case for this maser. In this case, the maser action is strong and the gain-bandwidth product is limited by the magnetic resonance linewidth.) For maser gains of about 14 dB, the ratio of the maser amplifier bandwidth to the magnetic resonance linewidth is approximately 0.5, and is the same for the ideal cavity maser and the traveling wave maser. For larger maser gains, the ideal cavity maser bandwidth is substantially less than the traveling wave maser bandwidth. For smaller maser gains, the ideal cavity maser bandwidth is greater than the traveling wave maser bandwidth. Therefore, a cavity maser with a 14-dB gain or less has good bandwidth potential if the magnetic Q is low.

C. Magnetic *Q*, Atomic *Q*, and External *Q*

The magnetic Q and atomic Q should now be computed to verify that we are in a regime of strong maser action, i.e., $Q_m << Q_a$. The value of magnetic Q can be calculated using

$$\frac{1}{Q_m} = \frac{2g^2\beta^2\mu_o}{h}\frac{I\Delta N\sigma^2\eta}{\Delta f_L} = 1.3\,(10^{-18})\,\frac{I\Delta N\sigma^2\eta}{\Delta f_L} \quad (6)$$

where Δf_L is expressed in MHz. A discussion of this equation is given in the Appendix and in [1].

The thermal equilibrium spin density population difference at 1.55 K can be calculated since the spins follow a Boltzmann population distribution. For a 0.05-percent chromium-doped ruby crystal oriented at the push–pull angle, the spin density population difference between levels 2 and 3 is $\Delta N = (0.144)(2.35 \times 10^{19}) = 3.38 \times 10^{18}$ spins/cc. The inversion ratio is approximately 2.0.

The filling factor for the cavity, η, must be estimated. The magnetic susceptibilty of the ruby for the signal transition (2–3) is essentially circularly polarized. The standing wave field in the cavity can be thought of as being half right circularly polarized and half left circularly polarized. Therefore, the maximum filling factor would be 0.50. Since some of the magnetic field extends beyond the ruby, the estimated filling factor is closer to 0.3.

For use in this formula, the signal transition should have a Lorentzian line shape. Since the natural linewidth of ruby is 60 MHz, some artificial broadening of the linewidth is necessary to achieve the goal of 85-MHz instantaneous bandwidth. This is accomplished with both a linear field gradient and single-step staggering. The linear field gradient is achieved by changing the length of the air gap between the hiperco pole pieces where the ruby is located. The single-step staggering is achieved with trim coils placed in the lid of the cavity structure.

Siegman has dicussed how the ratio of the maser amplifier bandwidth to the ruby resonance linewidth is improved with various types of stagger tuning. For a maser gain of 28 dB, the improvement with linear staggering and single-step staggering is comparable. In both cases, the maser bandwidth is approximately 80 percent of the resonance linewidth. Therefore, for an amplifier bandwidth of 85 MHz, the Lorentz equivalent linewidth is about 106 MHz.

The transition probability, $\sigma^2 = 0.9616$, can be determined from the spin Hamiltonian for ruby [3]. Substituting the above values in Eq. (6) gives a magnetic Q of 41. The atomic Q is roughtly 33,700 MHz/106 MHz, or 318. Therefore, $Q_m << Q_a$, as we assumed earlier. Using Eq. (4), the ratio of Q_e/Q_m for a 14-dB gain cavity is 0.66732. A magnetic Q of 41 implies an external Q of 27.

D. Overall Layout

A schematic drawing of the dual-cavity maser is shown in Fig. 1. As seen by the signal, the cavities are one-port reflection cavities with commercial WR-28 waveguide circulators used to separate the ingoing and outgoing signal. There is a waveguide transition between the circulator and the ruby cavities from the WR-28 waveguide to a reduced-height waveguide (WR-30). This was done to increase the coupling to the ruby cavity and will be discussed in the next section. The WR-30 waveguide has cross-sectional dimensions of 0.777 cm (0.306 in.) by 0.127 cm (0.050 in.). The second port of each cavity is beyond cutoff to the signal and is where the pump power (required to invert the ruby) is supplied to the cavity.

Experimentally, a single isolator between cavities did not provide enough isolation to prevent noticeable gain ripple. Therefore, two isolators were used. There are also waffle-iron bandpass filters in the output and input to keep the RF pump energy from reaching the HEMT post amplifier or escaping out the feedhorn. The ruby resonators are contained in the WR-10 waveguide, whose dimensions are 0.254 cm (0.10 in.) by 0.127 cm (0.050 in.). The 69.5-GHz pump energy is normally propagated in the WR-15 waveguide. Therefore, a waveguide transition from the WR-15 to the WR-10 waveguide was necessary. The coupling of the pump energy will be discussed in a later section. A photograph of the maser and HEMT post amplifier is provided as Fig. 2. An early photograph (showing only one interstage isolator) with part of the hiperco magnet return yoke removed is provided as Fig. 3.

III. Cavity Design

The magnetic Q of a cavity maser is determined by the maser material, its orientation relative to the dc magnetic field, the RF pumping scheme employed, the signal linewidth, and the bath temperature. The magnetic Q depends mostly on atomic parameters, and the cavity affects its value only through the polarization. The discrepancy between the desired and the actual polarization is accounted for with a "filling factor." To control the maser mid-band gain, the external Q is adjusted by changing the degree of coupling between the external line and the cavity. For stability, the positive external coupling must load the cavity more heavily than the negative resistance of the spin system [1].

The value of $Q_m = 41$ computed in the prior section indicates that the maser action is fairly strong. A strong external coupling, $Q_e = 27$, will therefore be required. In general, a coupling iris or aperture is used to

adjust the degree of coupling of the cavity to an external transmission line. When a cavity filled with a high dielectric-constant maser crystal is coupled to a waveguide, it is difficult to obtain the strong coupling required. The impedance mismatch between the maser crystal dielectric and the helium-filled waveguide may be large enough that sufficiently strong coupling can only be obtained with a coupling aperture consisting of one entire side of the cavity. This was the case with this maser. The role of the aperture is played by the helium-dielectric interface and the change in waveguide width.

The strength of the coupling can fall into one of three categories [4]:

(1) Reflection from the "aperture" dominates over that from the cavity; this is known as undercoupling.

(2) Reflection from the "aperture" cancels that from the cavity at the center frequency, and there is no reflected power; this is known as critical coupling.

(3) Reflection from the cavity dominates that reflected from the "aperture"; this is known as overcoupling.

The impedance locus on a Smith chart for these three cases is shown in Fig. 4. We are interested in the overcoupled case where the impedance locus encircles the origin. Microwave cavities may be considered from either a lumped equivalent circuit viewpoint or from the viewpoint of a transmission line with discontinuities. We will begin with a lumped-equivalent-circuit description, and then give a simple transmission-line equivalent circuit.

The principal advantage of the lumped-element model is that the various Q's are easily identified. We consider the circuit shown in Fig. 5. (The representation of the dielectric-filled cavity by a series resonant circuit and of the ruby spin system by a parallel resonant circuit is discussed in Siegman [1]. We have chosen to use the dual circuit, where the cavity is a parallel resonant circuit and the spin system is a series resonant circuit.) The quantities L, C, and G refer to the cavity inductance, capacitance, and conductance. The quantities L_m, C_m, and G_m refer to the ruby spin system. $G_e(Y_o)$ is the conductance (admittance) of the external transmission line that connects the cavity to the outside world. The reflection coefficient corresponds to the voltage gain and is given by

$$g(w) = \rho(w) = \frac{Y_o - Y_{load}}{Y_o + Y_{load}} \tag{7}$$

The expression for Y_{load} for the circuit of Fig. 5 is given by

$$Y_{load} = G + j\left(wC - \frac{1}{wL}\right) - \frac{1}{\left(\frac{1}{G_m} + j\left(wL_m - \frac{1}{wC_m}\right)\right)} \tag{8}$$

For a series resonance, the Q varies as wLG, and for a parallel resonance, the Q varies as $1/(wLG)$, where w is the angular frequency. The cavity and spin system angular resonance frequencies are denoted by w_o and w_a. The various Q's can now be identified as:

$$\begin{array}{lcll} \text{magnetic } Q & = & Q_m & = & 1/(G_m w_o L) \\ \text{external } Q & = & Q_e & = & 1/(G_e w_o L) \\ \text{atomic } Q & = & Q_a & = & w_a L_m G_m \\ \text{cavity } Q & = & Q_c & = & 1/(w_o L G) \end{array} \tag{9}$$

Substituting Y_{load} from Eq. (8) into Eq. (7) and using the definitions above, the voltage gain can be written as

$$g(w) = \frac{Q_m + \dfrac{Q_e}{1 + 2j\ Q_a\left(\frac{w - w_a}{w_o}\right)} - 2jQ_mQ_e\left(\frac{w - w_a}{w_o}\right) - \frac{G}{G_m}}{Q_m - \dfrac{Q_e}{1 + 2j\ Q_a\left(\frac{w - w_a}{w_o}\right)} + 2jQ_mQ_e\left(\frac{w - w_a}{w_o}\right) + \frac{G}{G_m}} \tag{10}$$

If $G << G_m$, then all specific admittances will drop out, and the gain is expressed solely in terms of the three quality factors, Q_e, Q_m, and Q_a. At resonance, $w = w_o$, and the voltage gain is given by

$$g(w) = \frac{Q_m + Q_e}{Q_m - Q_e} \tag{11}$$

The power gain is the square of this and is the result we used earlier as Eq. (3). Since the admittance levels are arbitrary, we set $G_e = 1$ mho ($R_e = 1$ ohm). Since the external Q must be 27, $w_o C = 27$. Therefore, $C = 1.275 \times 10^{-10}$ F. Since the resonant frequency is 33.68 GHz, $L = 1.75 \times 10^{-13}$ H. Since $Q_m = 41 = 1/(w_o L G_m)$, then $G_m = 0.666$ mho ($R_m = 1.5$ ohm). Since the atomic Q = 33,700 MHz/106 MHz = $318 = \omega_a L_m G_m$, then assuming $\omega_a = \omega_o$, $L_m = 1.00 \times 10^{-9}$ H and $C_m = 2.23 \times 10^{-14}$ F. The value of G is unspecified, but must be small compared to the value of G_m. We assume that $G = 0.05$ mho (R = 20 ohms), approximately an order of magnitude less than G_m. The values associated with the spin system, L_m, C_m, and G_m, are negative when the spin system is inverted.

A plot of the reflection coefficient using the program Touchstone[1] is shown in Fig. 6. Curve "a" shows the gain performance, and curve "b" shows the ruby absorption. The value of G_m for the absorption is decreased by a factor of 2 since the inversion ratio is about 2 for this frequency, ruby orientation, and RF pumping scheme. The ruby electronic gain is about 12.5 dB. The 3-dB bandwidth is about 82 MHz.

The same calculation can be plotted on a Smith chart to show the phase behavior (Fig. 7). Curve "a," which stays near the periphery of the chart, is the S_{11} behavior of the dielectric-filled cavity. The effect of the ruby spin system in an absorptive state, curve "b," can be seen to be quite strong where it crosses the resistance axis, that is, near resonance. For comparison, experimental data for an early ruby-filled cavity (where the spin system is not resonant) is shown in Fig. 8. (Although the center frequency of 33.0 GHz is slightly low, the frequency span is 2 GHz).

The aperture reflection coefficient can be estimated from a knowledge of the respective wave impedances [5]. In terms of the free space wavelength, λ, the ratio of the wave impedances (for transverse electric modes) for the ruby-filled WR-10 and the helium-filled WR-30 is given by

$$\frac{Z_2}{Z_1} = \left[\frac{\epsilon_1 - (\lambda/\lambda_{c_1})^2}{\epsilon_2 - (\lambda/\lambda_{c_2})^2}\right]^{1/2} = 0.31 \tag{12}$$

Therefore, the reflection coefficient ρ is given by

$$\rho = \frac{Z_2 - Z_1}{Z_2 + Z_1} = -0.53 \tag{13}$$

The change in wave impedance gives a substantial reflection coefficient. This was measured experimentally with the test fixture shown in Fig. 9. The tapered section between the alumina and the load material prevented reflection of the wave transmitted through the interface. The effect of the change in waveguide width is probably reduced because the ruby was pulled out 0.356 mm past the plane where the waveguide width changes. The experimental result is shown in Fig. 10. The impedance measurement was 15.9 ohms (relative to 50 ohms). Therefore, from Eq. (13), the corresponding reflection coefficient was -0.52 and essentially frequency-independent from 32 to 35 GHz.

Altman [6] has shown that an equivalent lumped-element resistor-inductor-capacitor (RLC) circuit with normalized parameters can be replaced by a circuit where the R, L, and C represent the intrinsic parameters of the cavity proper, if the effects of the coupling discontinuity are described by a transformer. In this case, the discontinuity or "aperture" is due to the dielectric material and the change in waveguide width. In more conventional cavities, it is due to a thin iris or coupling loop. It is an interesting theoretical experiment to model the present discontinuity as if it were simply a thin iris and to see where it leads. (This approach is not rigorous, and an electromagnetic field analysis is needed to derive the equivalent circuit.) Following the usual analysis for a thin iris in an otherwise homogeneous section of waveguide, the discontinuity can be represented by a transformer with a turns ratio given by

$$n^2 = \frac{1 + \rho}{1 - \rho} \tag{14}$$

where ρ is the reflection coefficient, assuming the output waveguide is matched. Using the reflection coefficient mentioned above, the turns ratio of the transformer is 0.56. A new lumped-element equivalent circuit incorporating the transformer can be constructed, where the new values of L', C', and R' representing the intrinsic cavity are

$$\begin{aligned} L' &= L/n^2 \\ C' &= n^2 C \\ R' &= R/n^2 \end{aligned} \tag{15}$$

and the circuit is shown in Fig. 11(a).

[1] Touchstone is a trademark of EEsof, Inc., Westlake Village, California.

This new parallel $R'L'C'$ circuit can be formally replaced by an equivalent transmission line. This is discussed in [7] and shown in Fig. 12. The admittance of the line can be determined by equating the susceptance slope parameter of the lumped circuit and the transmission line. The attenuation constant is related to the cavity conductance, G. The appropiate equations are

$$b = w_o C = \frac{1}{(w_o L)} = \frac{n\pi Y_o}{2}\left(\frac{\lambda_{g_o}}{\lambda_o}\right)^2 \qquad (16)$$

$$G = Y_o \alpha \ell \ (\alpha \text{ in nepers/unit length})$$

Since the physical transmission-line element in Touchstone is nondispersive, we assume $\lambda_{g_o}/\lambda_o = 1$. This leads to a Y_o of 2.7. Using $G = 0.05$, and $l = 0.2815$ cm, then $\alpha = 0.18$ dB/cm, or 0.051 dB per wavelength. The attenuation of the ruby-filled WR-10 waveguide was measured to be approximately 0.1 dB/cm, or 0.034 dB per guide wavelength at 33.7 GHz. Therefore, an approximate transmission-line equivalent circuit for the cavity can be constructed as shown in Fig. 11(b). A plot of the ruby absorption and gain for this circuit, using Touchstone, is shown in Fig. 6 as curves "c" and "d."

The ruby-filled waveguide is approximately one guide wavelength in length at 33.7 GHz. A full guide wavelength rather than a half was chosen so that the linear magnetic field taper required to broaden the ruby resonance linewidth would not be excessive. The resonant frequency of the cavity was adjusted by varying the length of the ruby crystal. The degree of external coupling was adjusted by pulling the ruby out past the plane where the waveguide changes width. Ruby paramagnetic resonance absorption plots were made at various magnetic field strengths with the cavity cooled to liquid nitrogen temperatures to determine the center frequency of the cavity at cryogenic temperatures. In addition, the tuning range of the maser is indicated by these plots. Such a plot is shown in Fig. 13.

IV. Magnet Design

The decision to build two cavities determined the volume over which the magnetic field must be provided. A circular region of 7.9-cm diameter was required to house the cavity structure and waveguides. The depth of the copper coil form upon which the superconducting wire was wound was estimated to be 19 mm. Therefore, the diameter of the region over which the hiperco yoke would operate is 11.7 cm (see Fig. 14). Assuming a roughly constant field strength of 12,400 G over this region, the total flux would be approximately (12,400 G) × (107.2 cm^2) = 1,329,280 G–cm^2.

If the hiperco annulus that provides the vertical return path for the magnetic field lines is 1.78 cm in the radial direction, the total magnet diameter will be 15.24 cm. The total cross-sectional area of the vertical return path at plane A–A (see Fig. 15) is 75.23 cm^2. Therefore, the field in the hiperco at this point (neglecting flux leakage outside the hiperco) is (1,329,280)/(75.2) = 17,677 G. The top and bottom plates of the hiperco yoke were chosen to be 2.03-cm thick. Therefore, the total cross-sectional area at plane B–B is 74.5 cm^2 and the field is 17,843 G. This is safely below the magnetic saturation for hiperco, which occurs at 23,600 G.

If the flux in the hiperco is 17,677 G, then from the B versus H curve of hiperco 27, the magnetizing force in the hiperco is about 40 Oe. Now the required number of ampere turns can be determined. Looking at a cross-sectional view of the magnet (Fig. 15), we can write Ampere's law for the contour drawn and find

$$\oint \vec{H} \bullet \vec{d\ell} = \frac{4\pi NI}{c} \qquad (17)$$

or

$$B(\text{gap})L(\text{gap}) + H(\text{hiperco})L(\text{hiperco}) =$$

$$22,854 \text{ G–cm} = \frac{4\pi NI}{c}$$

therefore

$$NI = \frac{(22,854 \text{ G–cm})(3 \times 10^{10} \text{cm/sec})}{4\pi(3 \times 10^9 \text{ esu/sec/A})}$$

$$= 18,187 \text{ A–turns} \qquad (18)$$

The coil form has an inside cross-sectional area of 15.24 mm × 16.51 mm = 2.52 cm^2. Assuming a wire cross-sectional area of 0.0613 mm^2 and a usable area (based on previous experience) of approximately 60 percent of 2.52 cm^2, or 1.51 cm^2, implies a total of (151 mm^2)/(0.0613 mm^2) = 2,462 turns, which means the current required will be I = (18,187)/(2462) = 7.4 A.

The total number of turns of NbTi superconducting wire actually wound on the coil form was 2,850 turns. This

implies a current requirement of 6.4 A. The actual current required to charge the magnet is about 6.5 A. The wire was epoxied in place on the coil form under vacuum using Scotchcast 235 epoxy.

The magnetic field over the rubies was broadened by machining a 1.8-deg linear taper in the round hiperco pole piece, which is located directly over the rubies. This taper broadened the ruby line width from 60 to 175 MHz. By rotating the pole piece, each ruby can be placed in a slightly different magnetic field. This technique could be used to achieve broader bandwidth at reduced gain if necessary. In this instance, the amplification bandwidth was set to approximately 85 MHz.

In addition to the main superconducting magnet, a set of four trim coils, two for each cavity, were wound on rexolite cores and placed into holes recessed in the cover of the cavity block. The rexolite cores were rectangular and measured 2.54 mm by 1.27 mm, and each coil was wound with 88 turns of copper wire. In practice, the current used to trim the ruby response is of the order of several hundred mA per coil. With 500 mA per coil, the total power dissipation is about 15 mW.

The main superconducting magnet was operated in the persistent mode by spot welding the free ends of the wire from the coil so the superconductor formed a closed loop. The spot weld was anchored to the negative terminal of a power supply, and the positive terminal was connected to the wire a few inches away. In the superconducting wire between these terminals, a small portion of the copper cladding was etched away, and a small coil of Nichrome heater wire was wound around the exposed NbTi wire. This portion of the wire was covered with Armstrong epoxy for strength and to thermally isolate the wire from the liquid helium. Approximately 60 mW of heater power was required to drive the wire normal. Components of the magnetic circuit can be seen in Figs. 2 and 3.

V. RF Pump Considerations

In order to invert the spin system, RF energy must illuminate the ruby. Since this ruby was oriented at the push–pull angle (c-axis angle of 54.735 deg to the dc magnetic field), a single pump frequency of 69.5 GHz was required. The RF pump energy was supplied by two Hughes solid-state (model 47134H) impact ionization avalanche transit time (IMPATT) oscillators. Each oscillator supplies over 100 mW of RF power. Although each oscillator comes equipped with its own waveguide ferrite isolator, it was found that additional isolators were required to prevent the oscillators from affecting each other.

The pump energy entered the cryostat in the WR-15 waveguide. After passing through an E-plane bend, the energy was passed to the WR-28 waveguide. The oversized waveguide was used to minimize the attenuation of the pump energy as it traveled 0.75 m to the maser. Just before reaching the maser, the waveguide switched back to WR-15. The two WR-15 waveguides were joined at a 3-dB sidewall hybrid coupler. The two outputs of the coupler went to the two cavities. The transitions from WR-15 to WR-28 were accomplished with commercially available cosine taper transitions.

The WR-15 waveguide entered the superconducting magnet and fastened directly to the maser cavity block. The cavity is one wavelength of a ruby-filled channel of WR-10, followed by a section of helium-filled WR-10 that acts as a waveguide beyond cutoff to the signal. A transition from WR-15 to the helium-filled WR-10 was necessary. Careful impedance matching of the pump waveguide to the ruby-filled cavities was necessary to keep the required RF pump power to a minimum.

The design of the quarter-wave step transformers used to impedance match the WR-15 waveguide to the WR-10 waveguide follows standard design [8,9]. The quarter-wavelength steps were first made in the waveguide height and then in the waveguide width. In each case, a two-section quarter-wave transformer was used (Figs. 16 and 17). In this analysis, Z_o and Z_3 are the impedances of the existing waveguides for which the transformers are being designed. The ratio R is given by

$$R = \frac{Z_o}{Z_3} \text{ or } \frac{Z_3}{Z_o} \tag{19}$$

whichever is greater than 1. The impedances of the intermediate quarter-wavelength steps, Z_1 and Z_2, are given by

$$\begin{aligned} Z_1 &= V_1 Z_o \\ Z_2 &= \left(\frac{R}{V_1}\right) Z_o \end{aligned} \tag{20}$$

where V_1 is given by

$$V_1^2 = \left(D^2 + R\right)^{1/2} + D \tag{21}$$

In this expression, D is given by

$$D = \frac{(R-1)\,k^2}{2(2-k^2)} \tag{22}$$

where k is given by

$$k = \sin\left(\frac{\pi B}{4}\right) \tag{23}$$

In this expression, B is the fractional bandwidth given by

$$B = \frac{2(\lambda_{gH} - \lambda_{gL})}{\lambda_{gH} + \lambda_{gL}} \tag{24}$$

where λ_{gH} and λ_{gL} are the guide wavelengths of the highest and lowest frequencies at which the transformer is to be operated. Using

$$Z_o = \frac{b}{a}\,\frac{\lambda_g}{\lambda_o} \tag{25}$$

for the impedance of a rectangular waveguide, the required height, width, and length (b, a, and L) of the quarter-wave steps can be determined. The length of all steps is one quarter-guide wavelength at 69.5 GHz. The results are shown in Table 2. Finally, a quarter-wavelength transformer of dielectric material with a dielectric constant approximately equal to 3 was used to match the helium-filled WR-10 to the ruby-filled WR-10.

VI. Performance

The electronic gain and ruby absorption of this maser at 1.5 K is shown in Fig. 18. The four magnetic-field trim coils have been adjusted for a flat response. The electronic gain is approximately 28 dB, and the 3-dB bandwidth is 85 MHz. The net gain is approximately 25 dB.

The noise temperature of each cavity can be calculated using [9]

$$T_{cav} = \frac{G-1}{G}\,\frac{hf}{k}\,\frac{G_{el}}{G_{net}}\,\frac{r}{r-1} + \frac{L_o}{G_{net}}\,\frac{1}{e^{hf/kT}-1} \tag{26}$$

where

G = gain of the maser = 316

G_{el} = electronic gain = 28 dB

G_{net} = net gain = 25 dB

L_o = forward loss = 3 dB

h = Planck's constant = 6.626×10^{-34} J-sec

f = frequency = 33.68×10^9 Hz

k = Boltzmann's constant = 1.38×10^{-23} J/K

T = bath temperature = 1.5 K

r = inverted spin population ratio = 3.76

where for push–pull pumping, r is given by

$$r = \frac{1 + 2I\left(N_2' - N_3'\right)}{1 - 2I\left(N_2' - N_3'\right)} \tag{27}$$

where

I = inversion ratio = 2.0

$N_i' = N_i/N$

where

N_i = number of spins in level i

N = total number of spins in levels 1, 2, 3, and 4

Using the values listed above, the noise temperature of a single cavity is 2.2 K. To calculate the noise temperature of the complete amplifier, the losses and gains and their physical temperatures in the circuit must also be known. These are shown in Fig. 19. We assume all the lines in the circuit are at the bath temperature. The noise contribution from a line with numerical insertion loss $L_i > 1$ referred to the input is given by

$$P_{input} = (L_i - 1)\,P_n(T) \tag{28}$$

where $P_n(T)$ is given by

$$P_n(T) = \frac{hfB}{e^{hf/kT} - 1} \tag{29}$$

If this line is preceeded by a lossy line of insertion loss $L_j > 1$ or an amplifier of gain $G > 1$, then the above expression is modified to

$$P_{input} = \frac{L_j\,(L_i - 1)\,P_n(T)}{G} \tag{30}$$

Therefore, the noise temperature of the complete amplifier can be written as

$$T_{maser} = (L_1 - 1)\,T_b' + L_1 T_{cav} + \frac{L_1\,(L_2 - 1)\,T_b'}{G_1}$$

$$+ \frac{L_1 L_2 T_{cav}}{G_1} + \frac{L_1 L_2\,(L_3 - 1)\,T_b'}{G_1 G_2} \qquad (31)$$

where T_b' is the effective noise temperature of the 1.5-K bath. It is defined by

$$T_b' = \frac{hf/k}{e^{hf/kT} - 1} \qquad (32)$$

Because of the reduced thermal noise emitted when $hf \approx kT$, the bath really appears to be 0.83 K. The sum of these five contributions yields a maser noise temperature at the cryogenic flange of 3.0 K.

Hot and cold load measurements performed at Goldstone, California, yielded a system T_{op} (outside the antenna) looking at the sky at zenith of 17.5 K. Subtracting 1.9 K for the cosmic background and 9.6–11.6 K for the atmosphere results in a noise temperature at the feedhorn input of 4–6 K. Subtracting 1.7 K for the feedhorn and gas seals and 0.3 K for the cooled waveguide components leads to a noise temperature at the cryogenic input of the maser of 2–4 K. This is consistent with the above calculated value of 3 K.

VII. Conclusion

A dual-cavity ruby maser has been built to support the Ka-Band Link Experiment conducted with the Mars Observer spacecraft. It operated in a superfluid helium bath with a physical temperature between 1.5 and 1.6 K. Its electronic gain was 28 dB; its net gain was 25 dB; the 3-dB instantaneous bandwidth was 85 MHz; and the noise temperature referred to the cooled feedhorn aperture was 5 K. The maser was installed in the pedestal room of the beam waveguide antenna at DSS 13.

Acknowledgments

The authors would like to thank Robert Clauss for many informative discussions during the development and implementation of this maser. Mark Fiore also provided theoretical and experimental support.

References

[1] A. E. Siegman, *Microwave Solid State Masers*, New York: McGraw-Hill Book Company, p. 259, 1964.

[2] J. R. Lyons, "Spin-Lattice Relaxation and the Calculation of Gain, Pump Power, and Noise Temperature in Ruby," *The Telecommunications and Data Acquisition Progress Report 42-98, vol. April-June 1989*, Jet Propulsion Laboratory, Pasadena, California, pp. 63–85, August 15, 1989.

[3] R. W. Berwin, "Paramagnetic Energy Levels of the Ground State of Cr+3 in Al_2O_3 (Ruby)," JPL Technical Memorandum 33-440, Jet Propulsion Laboratory, Pasadena, California, January 15, 1970.

[4] E. L. Ginzton, *Microwave Measurements*, New York: McGraw-Hill Book Company, p. 401, 1957.

[5] C. G. Montgomery, R. H. Dicke, and E. M. Purcell, eds., *Principles of Microwave Circuits*, London: Peter Peregrinus Ltd., p. 369, 1987.

[6] J. L. Altman, *Microwave Circuits*, Princeton, New Jersey: D. Van Nostrand Co., p. 214, 1964.

[7] G. Matthaei, L. Young, and E. M. T. Jones, *Microwave Filters, Impedance-Matching Networks, and Coupling Structures*, Dedham, Massachusetts: Artech House Books, p. 215, 1980.

[8] V. F. Fusco, *Microwave Circuits: Analysis and Computer Aided Design*, London: Prentice-Hall International, p. 306, 1987.

[9] J. S. Shell, R. C. Clauss, S. M. Petty, G. W. Glass, M. S. Fiore, J. J. Kovatch, J. R. Loreman, D. E. Neff, R. B. Quinn, and D. T. Trowbridge, "Ruby Masers for Maximum G/Top," accepted for *Proceedings of the IEEE*, May 1994.

Table 1. Gain stability versus number of cavities with 28-dB fixed total gain.

Number of cavities	Cavity gain, dB	ΔG for ΔT of 0.01 K, dB per cavity	Total ΔG, dB
1	28	0.51	0.51
2	14	0.095	0.19
3	9.33	0.0511	0.15
4	7	0.035	0.14

Table 2. Design parameters and step sizes for the WR-15 to WR-10 transitions.

Parameter	WR-15 to RH WR-15	RH WR-15 to WR-10
R	1.48	2.30
B	0.20	0.20
k	0.156	0.156
D	$2.96(10^{-3})$	$8.00(10^{-3})$
V_1	1.104	1.235
b_1	1.40 mm	1.27 mm
b_2	1.70 mm	1.27 mm
a_1	3.76 mm	3.30 mm
a_2	3.76 mm	2.72 mm
L_1	1.32 mm	1.42 mm
L_2	1.32 mm	1.78 mm

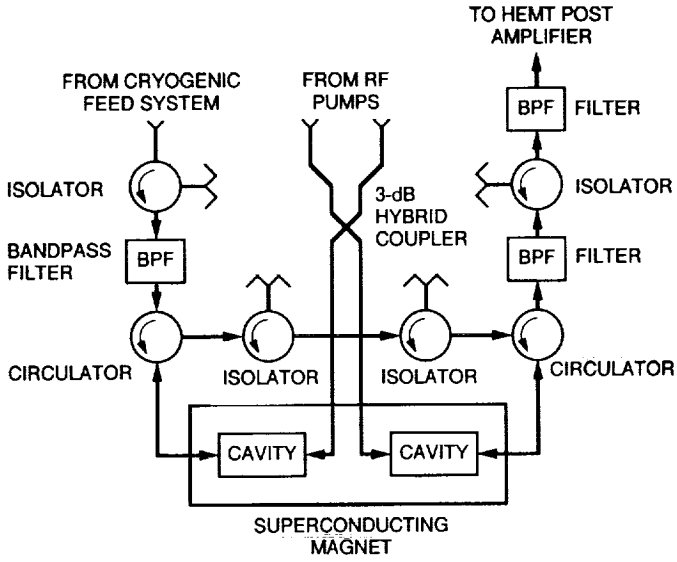

Fig. 1. The dual-cavity maser.

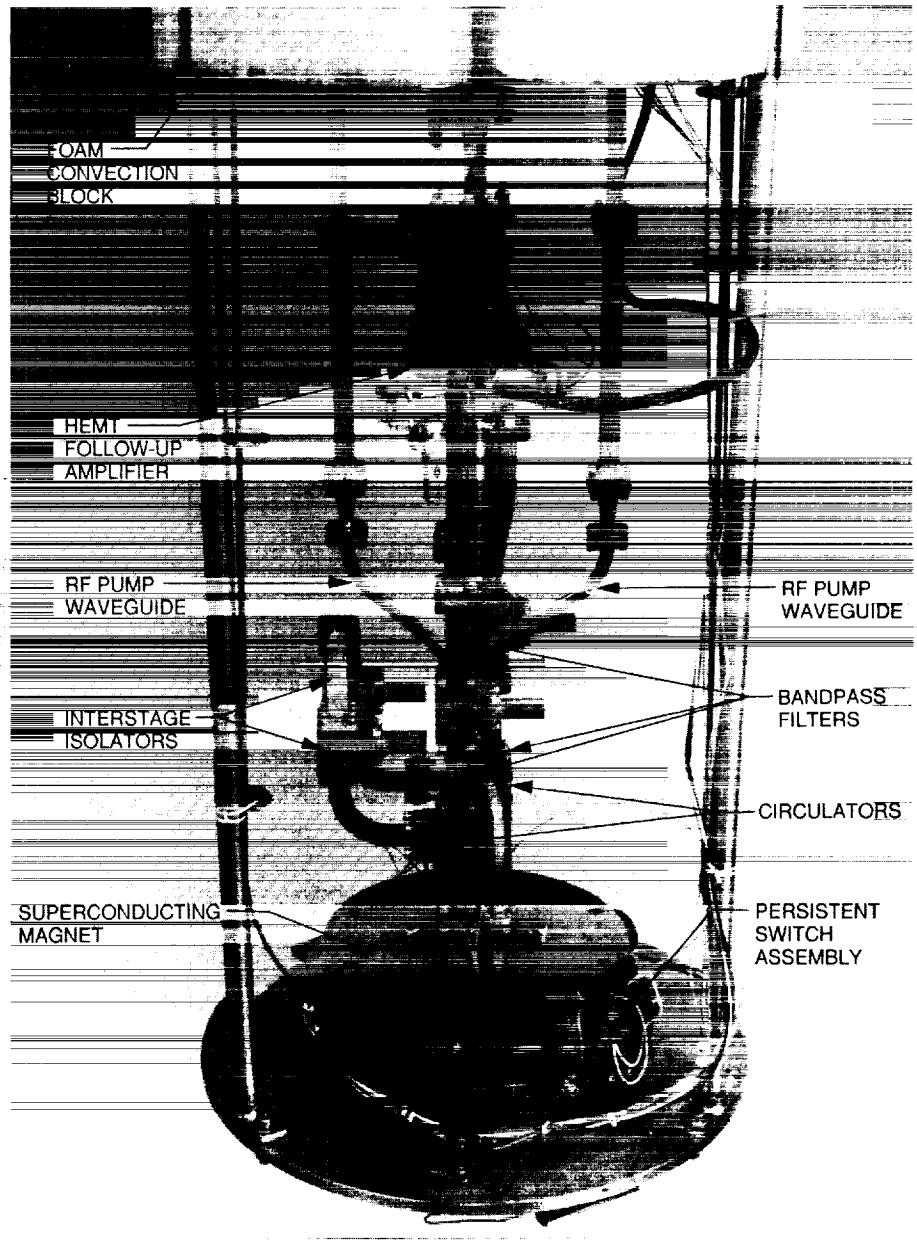

Fig. 2. The cryogenic portion of the completed maser and HEMT post amplifier (the helium dewars and room temperature components are not shown).

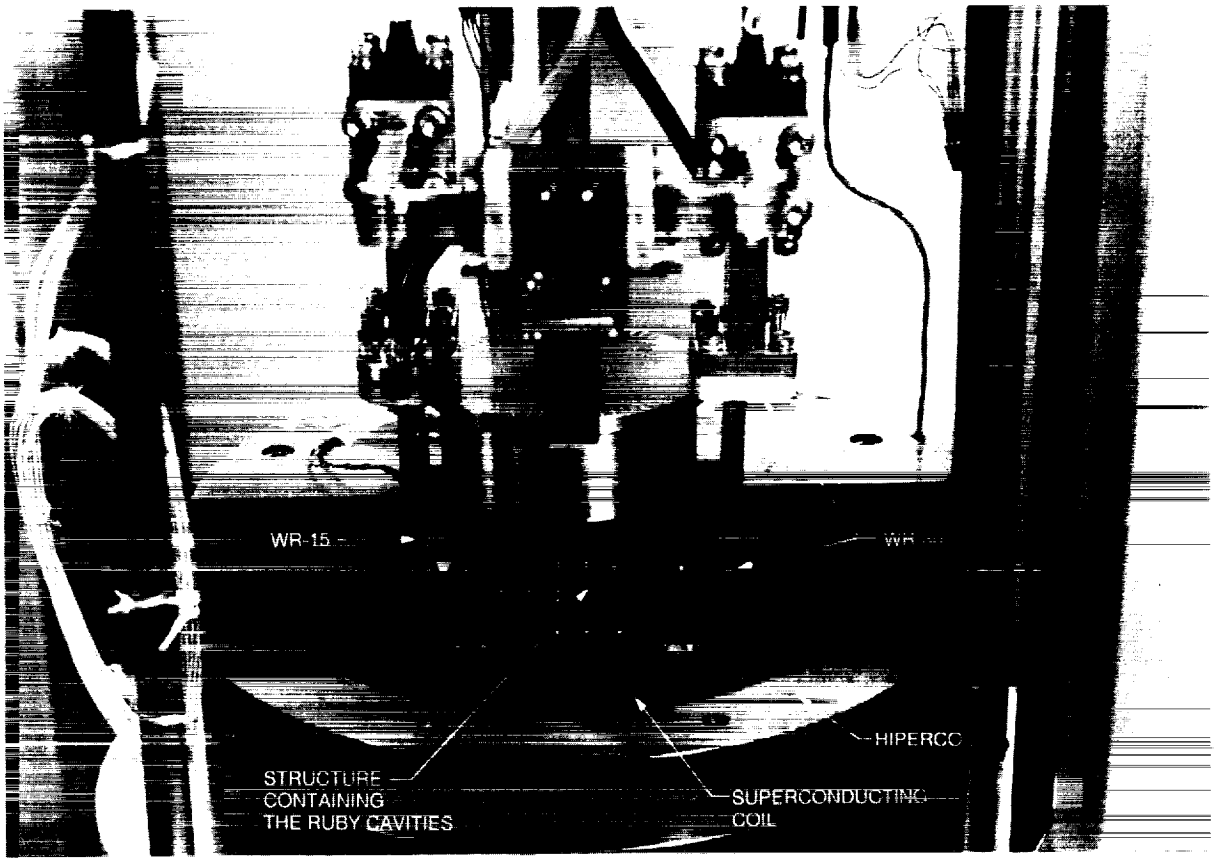

Fig. 3. A view of the maser with half of the top magnet pole piece removed and the round hiperco plug raised to expose the copper superconducting coil form and the structure containing the maser cavities. (At the time of this photograph, only one interstage isolator was present, and the trim coils were not yet installed.)

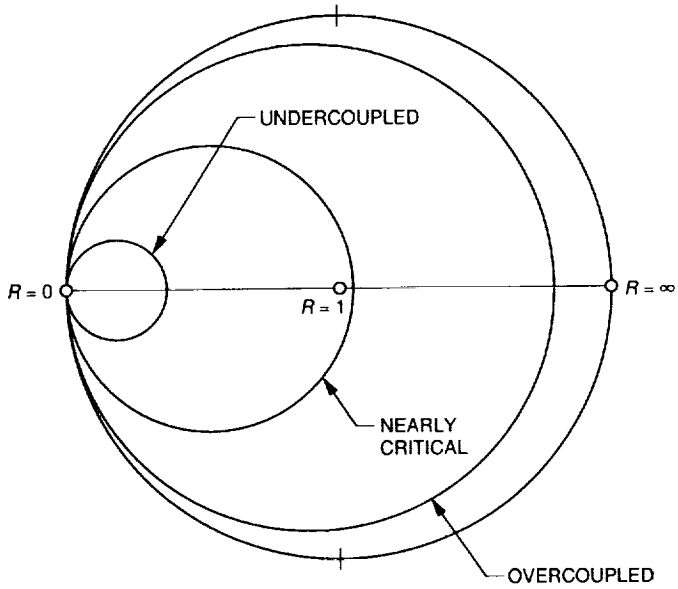

Fig. 4. The reflection coefficient behavior on a Smith chart display of undercoupled, critically coupled, and overcoupled cavities.

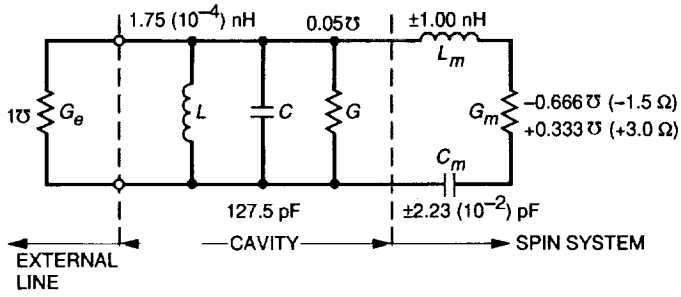

Fig. 5. A lumped-element model of one of the ruby maser cavities.

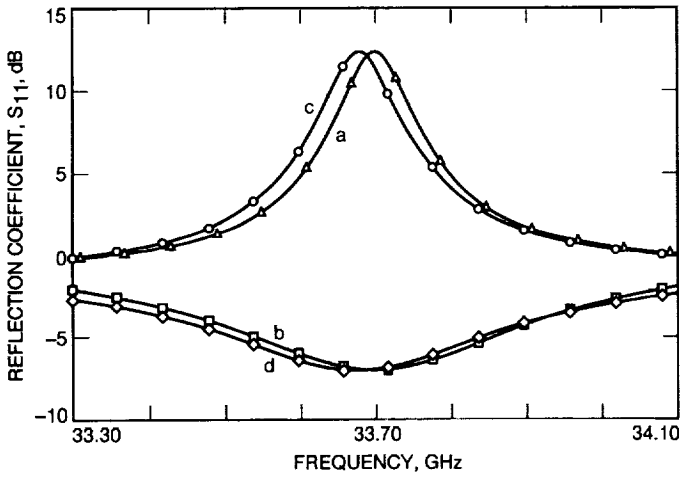

Fig. 6. Calculated ruby absorption and gain in dB versus frequency. Curves "a" and "b" are computed from the lumped-element model of Fig. 5. Curves "c" and "d" are from the transmission-line model of Fig. 11(b).

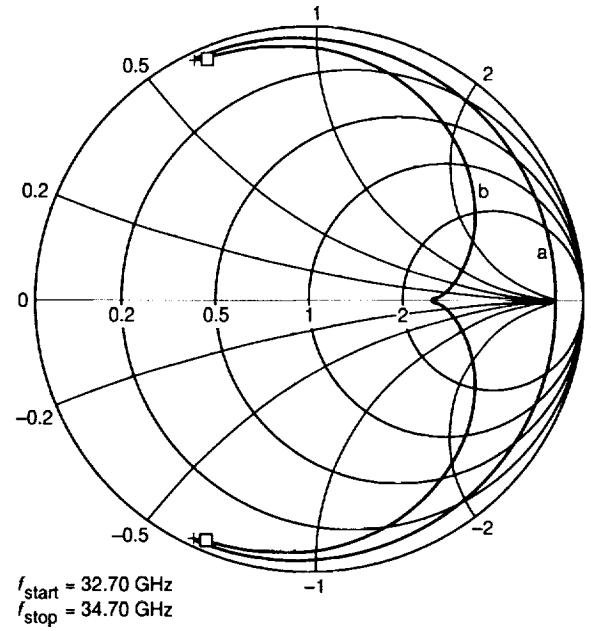

Fig. 7. A Smith chart display of the scattering coefficient (S_{11}) response of the lumped-element parallel RLC cavity model of Fig. 5 (curve "a"), and a similar display with the addition of the series RLC network representing the spin system in a dissipative state (curve "b").

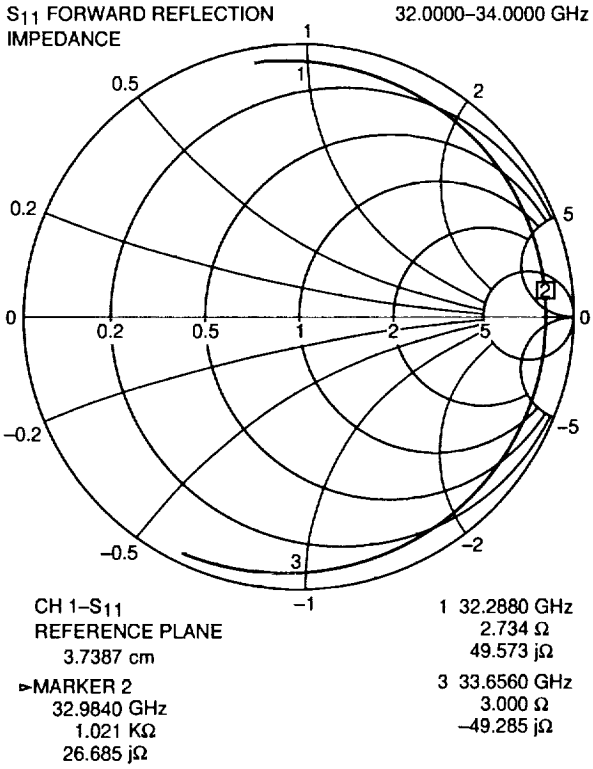

Fig. 8. Measured room temperature reflection coefficient data of one of the ruby cavities (before final adjustment of the resonant frequency).

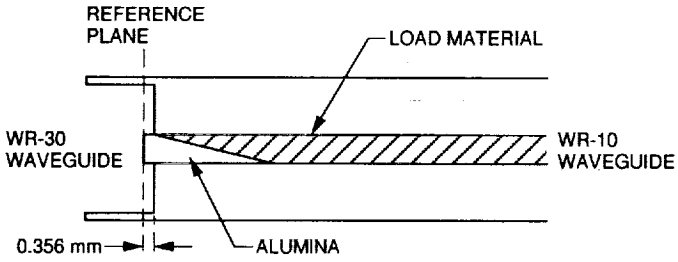

Fig. 9. The test fixture used to measure the reflection coefficient from the cavity aperture (air–ruby interface and WR-30-to-WR-10 transition).

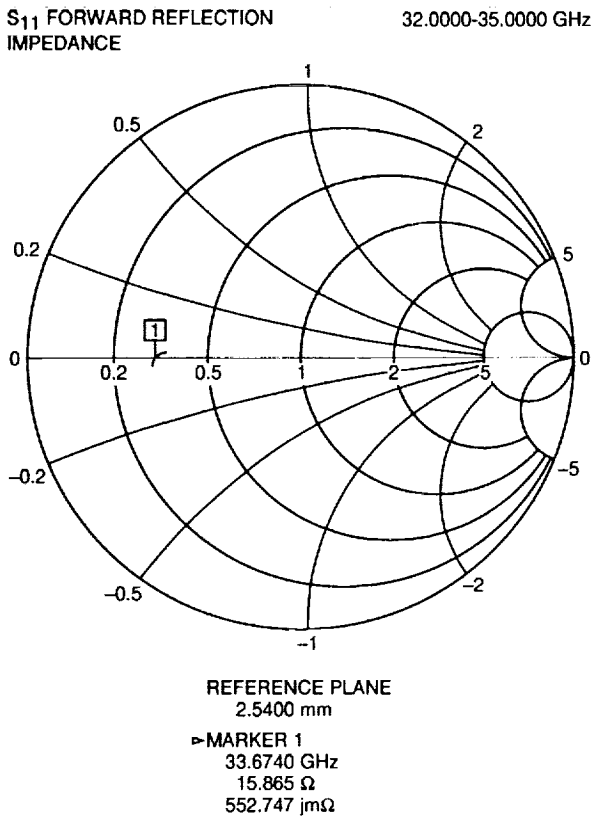

Fig. 10. Measured reflection coefficient, S_{11}, of the test fixture in Fig. 9 from 32 to 35 GHz.

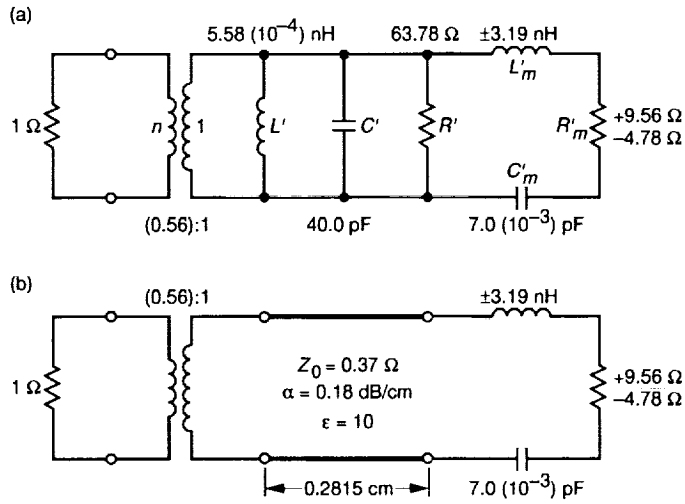

Fig. 11. Modified lumped-element model of the cavity (a) incorporating a transformer to represent the aperture and (b) the same circuit with the parallel RLC circuit replaced by its transmission-line equivalent.

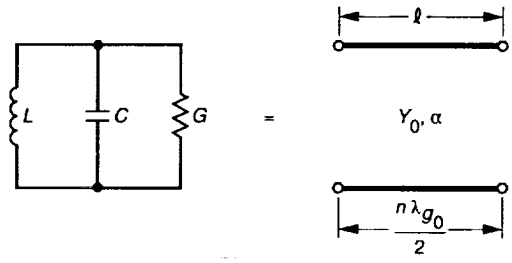

Fig. 12. The equivalence used to replace the parallel RLC lumped-element model of the cavity with a transmission line.

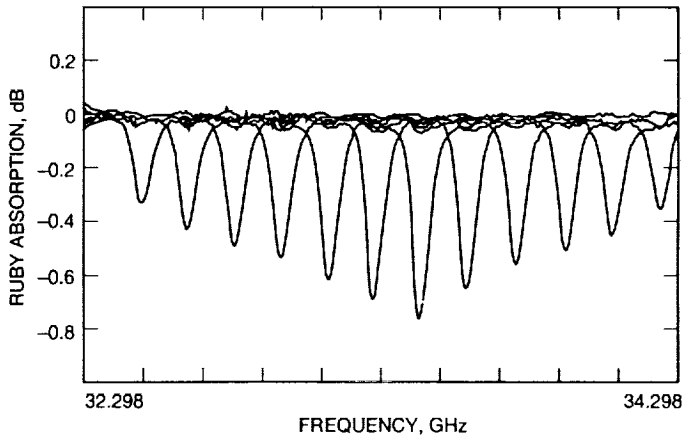

Fig. 13. Ruby absorption versus frequency for different values of the external magnetic field. The cavity was near liquid nitrogen temperatures (77 K).

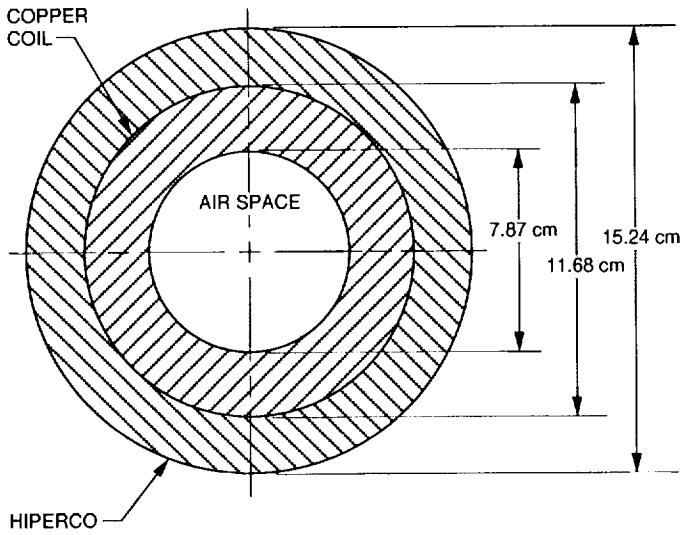

Fig. 14. Cross-sectional view of the magnet assembly, including the hiperco magnet yoke, superconducting coil, and air space for the ruby cavities.

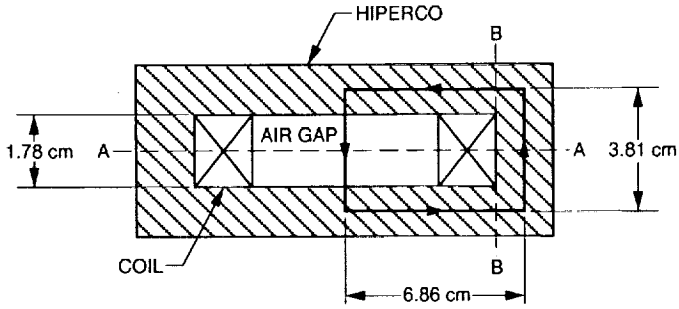

Fig. 15. The transverse dimensions of the magnet assembly, including the contour used for the Ampere's law integration.

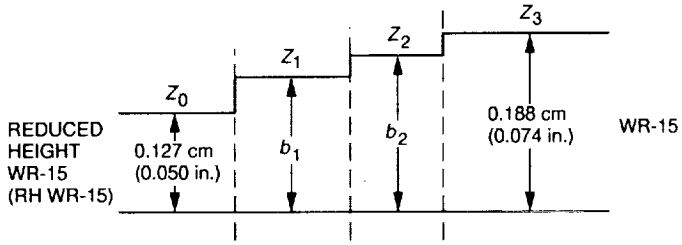

Fig. 16. The impedances and heights to be calculated in the quarter-wave transformer matching of the WR-15 waveguide to the reduced-height WR-15 waveguide. (Height and length values are given in Table 2).

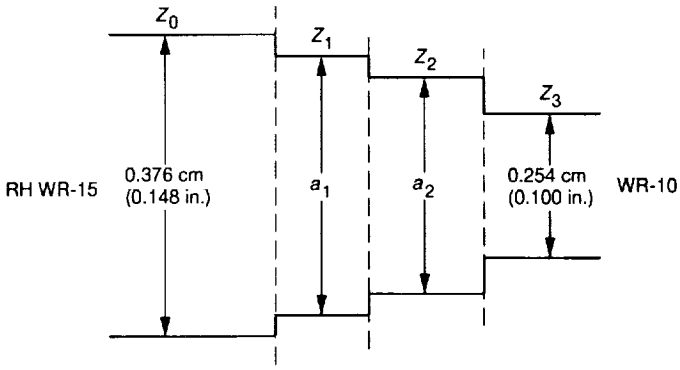

Fig. 17. The impedances and widths to be calculated in the quarter-wave transformer matching of the reduced-height WR-15 waveguide to the WR-10 waveguide. (Width and length values are given in Table 2).

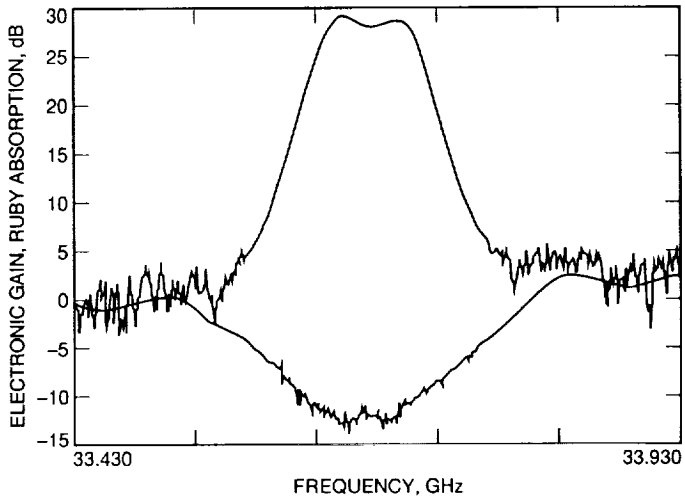

Fig. 18. Ruby gain and absorption versus frequency for the completed dual-cavity maser.

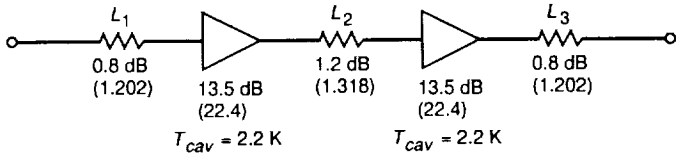

Fig. 19. Loss and gain elements used to estimate the noise temperature of the complete dual-cavity maser at the cryogenic flange.

Appendix

Equation 6 for the magnetic Q is given as

$$\frac{1}{Q_m} = \frac{2g^2\beta^2\mu_o}{h}\frac{I\Delta N\sigma^2\eta}{\Delta f_L} \qquad \text{(A-1)}$$

This expression is correct for m–kg–sec (MKS) units, where

$\beta = 9.27 \times 10^{-24}$ J/T (Bohr magneton)

$\mu_o = 1.26 \times 10^{-6}$ H/m

$h = 6.626 \times 10^{-34}$ J–sec

$g = 2.0$ (g-factor of the electron)

$\Delta N =$ thermal equilibrium spin density population difference for the signal transition, spins/cc

$\Delta f_L =$ resonance linewidth, MHz

$I =$ inversion ratio (dimensionless)

$\sigma^2 =$ transition probability (dimensionless)

$\eta =$ filling factor (dimensionless)

If the same equation is to be evaluated using cm–g–sec (CGS) units, where

$\beta = 9.27 \times 10^{-21}$ ergs/G

$\mu_o = 1$ G/Oe

$h = 6.626 \times 10^{-27}$ erg–sec

then an additional factor of 4π is necessary in the numerator. This is due to the fact that magnetic susceptibility, χ, in MKS and CGS units are given by

$$\chi = \left(\frac{\mu}{\mu_0} - 1\right) \quad MKS \qquad \text{(A-2)}$$

$$\chi = \frac{\mu - 1}{4\pi} \quad CGS \qquad \text{(A-3)}$$

where μ/μ_o is the relative permeability in the MKS case and μ is the relative permeability in the CGS case.

Therefore, setting $\mu_o = 1$ in Eq. (A-2) is not the same as the CGS definition in Eq. (A-3). Since the inverse magnetic Q is essentially the same as the magnetic susceptibility [1], the numerator must have an additional factor of 4π when the other variables are expressed in CGS units. There is an additional factor of 1.0×10^{-6} in the numerator for the CGS case when converting from Hz to MHz. This same factor does not appear in the MKS case because the conversion from Hz to MHz is compensated for by the conversion from spins/m^3 to spins per cm^3.